

Engineering edge states in topoelectric circuits

Anish Kuanr,^{*} Rajashri Parida,[†] Saralasarita Mohanty,[‡] and Tapan Mishra[§]

School of Physical Sciences, National Institute of Science Education and Research, Jatni 752050, India and Homi Bhabha National Institute, Training School Complex, Anushaktinagar, Mumbai 400094, India

(Dated: March 3, 2026)

We study the topological phase transition in a two-leg Su-Schrieffer-Heeger (SSH) ladder by re-defining the unit-cell structure. For both identical hopping dimerization pattern (uniform) and alternate hopping dimerization pattern (staggered), we demonstrate that different unit-cell choices generate different topological phases and phase transitions. In the uniformly dimerized ladder, variation of the inter-leg coupling induces transitions between distinct topological phases mediated by a gapless region. In contrast, the staggered dimerization configuration exhibits a richer phase structure, supporting both topological-topological and trivial-topological transitions occurring through a single gap-closing point, depending on the unit-cell definition. The phases are characterized through bulk-boundary correspondence, edge-state analysis, and bulk invariant. These analyses reveal interesting phenomena, including regimes supporting four localized boundary modes in the weak inter-leg coupling limit and two boundary modes in the strong inter-leg coupling limit. We further perform an experimental implementation using topoelectric circuit simulation by mapping the lattice Hamiltonian to an equivalent LC circuit. Circuit impedance and voltage responses obtained from LTspice simulations confirm the predicted edge-state signatures. These results establish topoelectrical platforms as experimentally accessible realizations of tunable lattice topological phases.

I. INTRODUCTION

The concept of topology has profoundly reshaped our understanding of quantum phases of matter by revealing states that cannot be characterized within the traditional Landau paradigm of symmetry breaking and local order parameters. Instead, topological phases are distinguished by global invariants leading to robust boundary modes that persist against local perturbations as long as certain symmetries are preserved. These features are collectively captured under the notion of symmetry-protected topological (SPT) phases, which have become a central theme in modern condensed matter physics due to their simplicity in terms of short-range entanglement structure, conceptual richness, and technological potential. Among the simplest and most instructive models realizing an SPT phase is the one-dimensional Su-Schrieffer-Heeger (SSH) model [1], where dimerized nearest-neighbor hopping amplitudes give rise to a topological phase transition from a trivial insulating phase as the hopping dimerization is appropriately varied. Despite its minimal structure, the SSH model has served as a versatile platform for exploring fundamental aspects of topology, including bulk-boundary correspondence, quantized geometric phases, topological transport, and topological phase transitions. Its conceptual simplicity has enabled direct experimental realizations across a wide range of systems, including ultracold atoms, photonic and acoustic lattices, mechanical metamaterials, superconducting platforms, and, more recently, electrical circuits [2–18].

A richer landscape emerges when moving beyond strictly one-dimensional chains to quasi-one-dimensional geometries such as ladders. Ladder systems provide a natural setting to investigate the dimensional crossover by interpolating between one and two dimensions and host new physical mechanisms stemming from inter-chain coupling and proximity effects. In the context of coupled SSH chains, various systems have been explored in the topological ladder settings to understand the role of inter-chain coupling on the topological character of the system. Recent studies have shown that when two identical SSH chains of topological configuration are coupled with each other, the inter-chain coupling immediately destroys the topological nature of the system. However, when one topological and one trivial chain are coupled, then there occurs a topological to trivial phase transition as a function of the inter-leg coupling. It has also been shown that when an SSH chain of either topological or trivial character is coupled with a chain of uniform hopping, a topological phase can be induced by the inter-chain hopping. These emergent topological phase transitions reveal the peculiar role of inter-leg couplings in ladder systems [19]. It is to be noted that the onset of topological phases in such coupled SSH chains are found to be due to the emergence of effective SSH-type chains which satisfies either topological or trivial configuration, depending on the choice of hopping strengths involved. The hallmark signature of the SPT phases in SSH type lattices is the presence of the bulk-boundary correspondence that associates bulk topological invariants with certain zero-energy edge states in the system with open boundaries. For example the topological phase for an SSH chain exhibits two degenerate edge states localized at the two end sites of the lattice. These features of the open boundary system strictly depend on the choice of unit cells of the periodic system. While such a choice is limited in an SSH

^{*} anish.kuanr@niser.ac.in

[†] rajashriparida33@gmail.com

[‡] saralasarita@niser.ac.in

[§] mishratapan@gmail.com

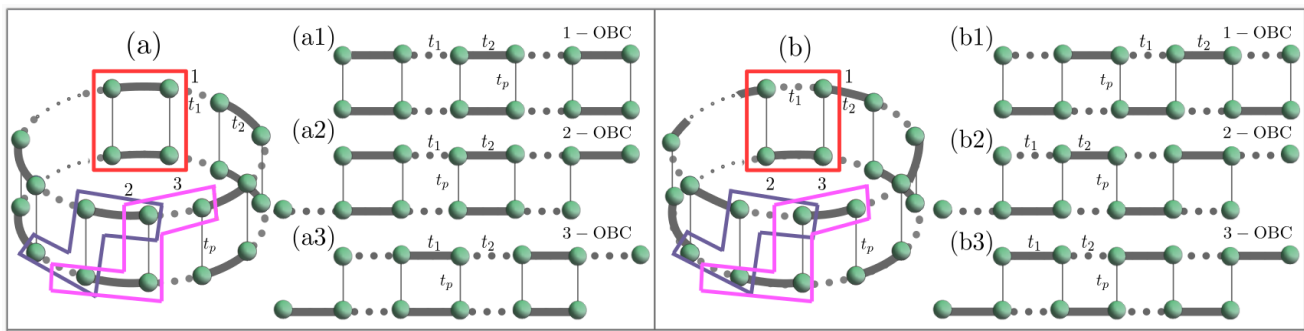


FIG. 1. Schematic of two types of ladder configurations. The left (right) panel indicates the ladder in uniform (staggered) configuration. The red, blue, and magenta boxes highlight three possible unit cell configurations in both cases, which give rise to different edge structures as shown in the bottom panels.

chain, coupled SSH chains platforms provide a versatile ground to achieve topological phases and the edge states by leveraging the dimensionality to construct different types of unit cells. For example, for the two-leg SSH ladder, a completely different scenario appears. It has been shown that when the ladder is in the topological phase, the edge states appear at the two end sites of any one of the legs when the OBC is achieved by vertically cutting the ladder. This highlights the enhanced flexibility to manipulate the edge states when one moves from purely 1D chain to ladder geometries.

Motivated by this, in this work we explore possible route to construct different unit cells in a two-leg ladder SSH model to engineer different topological phases and their associated edge states. We start from the two possible configurations; (i) uniform dimerization and (ii) staggered dimerization as shown in the left and right panels, respectively, of Fig. 1. We show that if different types of unit cells are chosen (demarcated as blue and magenta boxes) for both the uniform and staggered dimerization cases, then an interesting topological landscapes emerge. We reveal that for the uniform dimerization case (left panel), for both the blue and magenta unit cell choices, the system exhibits a topological to topological phase transition through a gapless region as the rung hopping is varied. However, for the staggered dimerization case, a much richer scenario emerges. For the unit cell marked by the blue box, the system exhibits a topological to topological transition, and for the magenta unit cell, a trivial to topological phase transition as a function of the rung hopping. Unlike the uniform dimerization case, here the transitions occur through gap closing points instead of the gap closing region. We quantify these topological phases and transitions through the signatures from the bulk-boundary correspondence. Interestingly, we obtain that, while all the topological phases exhibit the standard bulk-boundary correspondence of a two-leg ladder that dictates two localized edge modes, in the case of staggered dimerization, the topological phase corresponding to the blue unit cell exhibits four edge states when the inter-leg coupling is weak. In the end, we propose an ex-

perimental realization of our findings through topoelectric circuit implementation of the model under consideration. By utilizing the impedance and voltage responses we demonstrate the realization and engineering of edge states in SSH ladder systems.

II. MODEL

We consider a system of non-interacting spinless fermions on a two-leg ladder, where each leg individually exhibits SSH model type hopping dimerization as depicted in Fig. 1. The model that describes such a system is given by the Hamiltonian

$$H = - \sum_j \left[t_a - (-1)^j \alpha_a \right] \left(a_j^\dagger a_{j+1} + \text{H.c.} \right) - \sum_j \left[t_b - (-1)^j \alpha_b \right] \left(b_j^\dagger b_{j+1} + \text{H.c.} \right) + H_i. \quad (1)$$

where H represents the Hamiltonian of non-interacting spinless fermions

$$H_i = \begin{cases} -t_p \sum_j \left(a_j^\dagger b_j + \text{H.c.} \right) & \text{for unit cell 1} \\ -t_p \sum_j \left(a_j^\dagger b_{j+1} + \text{H.c.} \right) & \text{for unit cell 2 and 3} \end{cases} \quad (2)$$

$a_i (a_i^\dagger)$ and $b_i (b_i^\dagger)$ are the particle annihilation (creation) operators on leg-a and leg-b, respectively, where i represents the rung index. t_a and t_b are the hopping amplitudes along the legs and α represents the modulation parameter that dictates the hopping dimerization. t_p represents the inter-leg hopping amplitude which is also called the rung hopping.

The ladder system possesses two distinct dimerization patterns. (i) Uniform dimerization configuration, where both the SSH legs of the ladder are in the same phase, being either topological or trivial, as illustrated in the left panel of Fig. 1, (ii) staggered dimerization configuration,

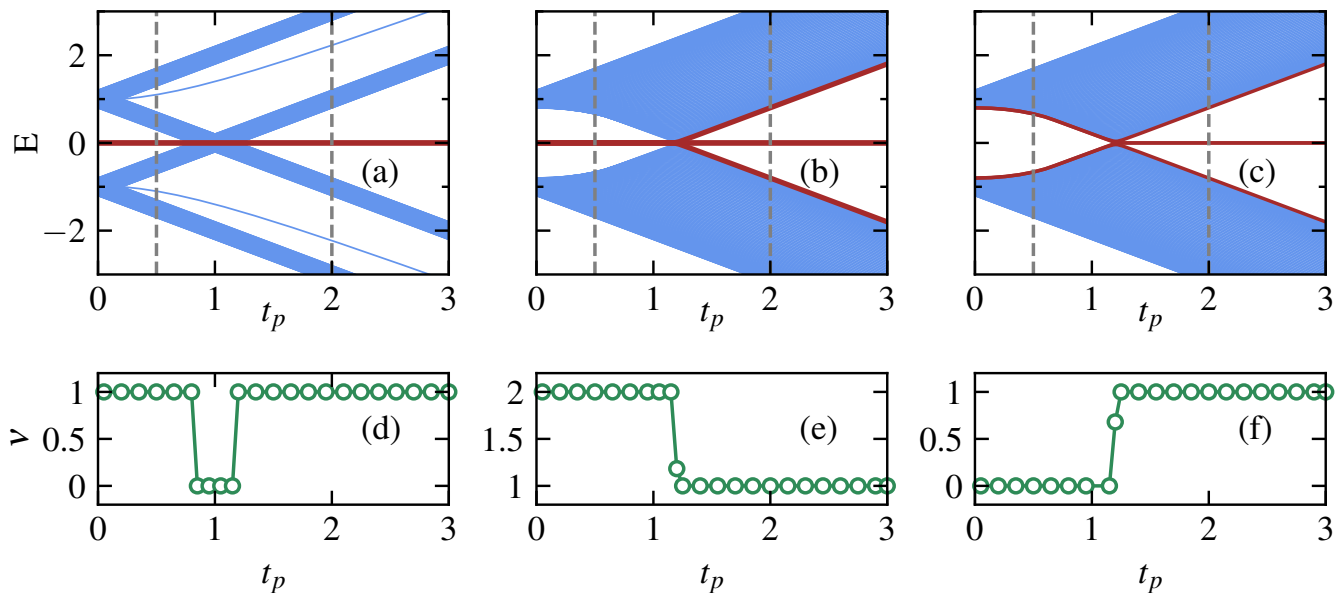


FIG. 2. Energy spectra of a two-leg ladder as a function of the inter-leg hopping strength t_p . Panel (a) shows the energy spectrum when both chains are in the staggered dimerization configuration. Panels (b) and (c) show the energy spectrum for ladders with uniform dimerization on both chains, corresponding to $(t_1, t_2) = (0.2, 1.0)$ and $(1.0, 0.2)$, respectively. The system size is $L = 200$ sites. Panels (g)–(h) show the corresponding winding number ν/π as a function of t_p for the parameter regimes shown in panels (a)–(c). The isolated states in (a) are the edge states in the high energy gaps.

where one leg of the ladder is in the topological phase while the other remains in the trivial phase, as shown in the right panel of Fig. 1.

To realize the two dimerization patterns discussed above, we choose the following parameter settings. The uniform dimerization configuration is obtained by taking equal hopping amplitudes along the two legs, $t_a = t_b = t$, and identical modulation strengths, $\alpha_a = \alpha_b = \alpha$. In contrast, the staggered dimerization configuration is implemented by choosing equal hopping amplitudes, $t_a = t_b = t$, but opposite modulation strengths, $\alpha_a = -\alpha_b = \alpha$. Throughout this work, we fix $t = 0.6$ and $\alpha = 0.4$, which yield the strong and weak bond amplitudes $t_1 = t + \alpha = 1.0$ and $t_2 = t - \alpha = 0.2$, respectively, along each legs of the ladder.

Due to the peculiarity of the ladder structure, it is possible to define different unit cells. For both dimerization patterns, three different choices of unit cells are marked as considered, as highlighted by the red, blue, and magenta boxes in Fig. 1(a) of both the left and right panels. In the following we will show that each such choice of unit cell leads to different topological features. We analyze the topological properties corresponding to all these configurations and demonstrate how such choices can lead to different edge states realizations under OBC. Then we obtain signatures of edge states from the electric circuit simulations.

III. RESULTS

We analyze the topological properties of the two-leg SSH ladder model by studying the real-space energy spectrum of the Hamiltonian shown in Eq. 1 under OBC together with the corresponding bulk topological invariant for an equivalent periodic system. The topological properties of coupled SSH ladders under OBC, specifically when both chains are in the topological phase (a uniform dimerization case) or when one chain is topological and the other trivial (a staggered dimerization case), and are coupled via perpendicular interleg hopping, have been discussed previously by some of us in Ref. [20]. When both chains are topological, two pairs of zero-energy edge modes appear in the decoupled limit. However, upon turning on the perpendicular rung hopping, these modes hybridize and move away from zero energy, rendering the topology weak. For unit cell 1 with both chains initially in the trivial phase, no zero-energy edge states are present, and the bulk properties remain identical to the case where both chains are topological, as both configurations share the same bulk spectrum (not shown). On the other hand, in the staggered dimerization case, unit cell 1 is known to exhibit a topological phase transition accompanied by the emergence of a pair of zero-energy edge states. A shift of this unit cell by one rung leaves the bulk Hamiltonian invariant but restores reflection symmetry about the horizontal axis. As a result, the bulk physics remains unchanged, while the location of edge states changes from one leg of the ladder

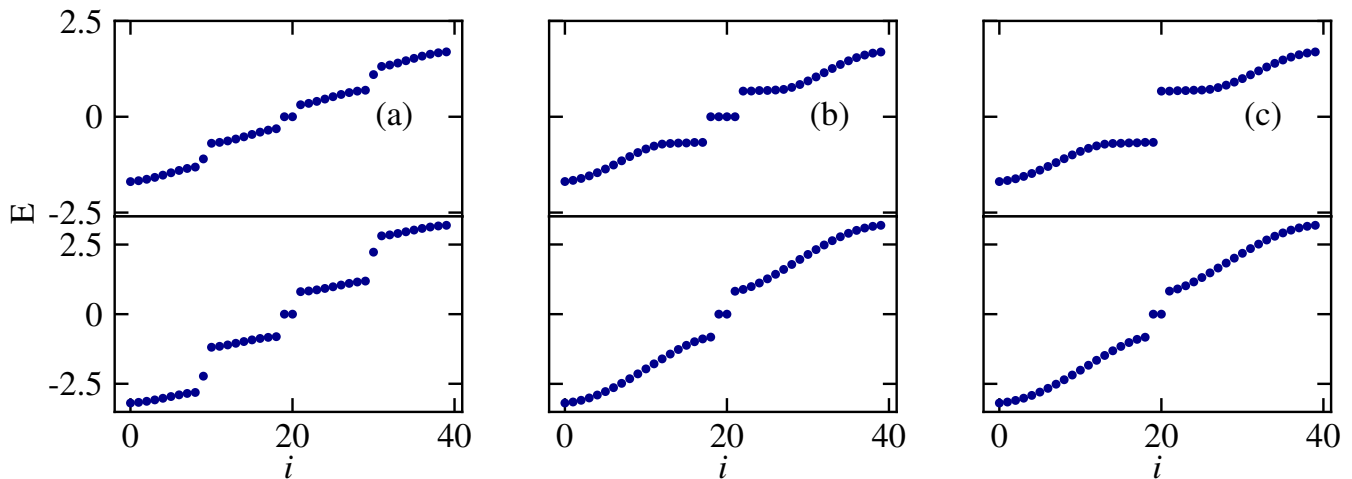


FIG. 3. The energy spectra E as a function of the eigenstate index (i) for two representative cuts, $t_p = 0.5$ and $t_p = 2.0$ corresponding to grey dashed lines in Fig. 2(a)–(c).

to the other. This phenomenon has been discussed in detail in Ref. [20].

In this work, we consider different unit cells (2 and 3) as depicted in the Fig. 1. In the case of uniform dimerization (left panel of Fig. 1) the unit cells 2 and 3 are related by a reflection symmetry and are equivalent to each other. However, for the staggered dimerization case, such equivalence is absent. Therefore, we focus only on unit cell 2 for the former case and on 2 and 3 for the latter. The real-space energy spectra as functions of inter-leg hopping t_p are shown in Fig. 2(a) for unit cell 2 of the uniform dimerization configuration and in Fig. 2(b) and (c) for unit cells 2 and 3, respectively, of the staggered dimerization configuration. All calculations are performed for a system of $L = 200$ sites, with fixed hopping amplitudes $t_1 = 1.0$ and $t_2 = 0.2$. We obtain that for all the three cases, the system exhibits a gapped to gapped phase transition as a function of t_p at half filling of the band (central white regions). While for the uniform dimerization case, the gapped to gapped transition occurs through a gap closing region (Fig. 2), for the staggered dimerization case, the transition occurs through a gap closing point (t_p^c) for both the unit cell configurations (Fig. 2 b and c). It is to be noted that, in all the cases the spectrum exhibits states at zero energies (marked as red) inside the gapped region(s).

To identify the number of zero-energy states, we plot the real-space energy spectrum as a function of the site indices (i) for two representative cuts of t_p in Fig. 2(a)–(c), i.e. $t_p = 0.5$ and 2.0 chosen within the gapped phases on either sides of the bulk gap closing which are shown in the upper and lower panels, respectively, of Fig. 3(a)–(c). For the uniform dimerization case [Fig. 3(a)], two zero-energy states persist on both sides of the gap closing. In contrast, for unit cell 2 of the staggered dimerization configuration [Fig. 3(b)], four zero-energy states appear for $t_p < t_p^c \sim 1.2$. However, in the gapped phase for

$t_p > t_p^c \sim 1.2$, only two states with zero energy survive [Fig. 3(b) (lower panel)]. For unit cell 3 [Fig. 3(c)], no zero-energy states appear within the gap for $t_p < t_p^c \sim 1.2$ (upper panel). However, beyond the gap closing point ($t_p > t_p^c \sim 1.2$), a pair of zero-energy states emerges in the gap (lower panel). The appearance of such the zero energy states within the bulk gap are typical signatures of edge states in topological phases.

In order to characterize the zero-energy states appearing here, we calculate the on-site probability densities for a system of $L = 40$ sites. For this demonstration, we only choose the case of unit cell 2 of the staggered dimerization case (Fig. 2(b)) and plot the onsite probability densities $|\psi_i|^2$ at each sites for $t_p = 0.5$ and $t_p = 2.0$ in Fig 4 (a) and (b), respectively. These also correspond to the states shown in Fig. 3(b) upper and lower panels. The lattice sites are represented by circles, and the face colors indicate the on-site probability densities. All the four zero energy states are clearly localized at the edge sites for $t_p = 0.5$ as shown in Fig 4(i-iv), indicating that all of them are edge states of the system. On the other hand, only two states are localized at the edge sites for $t_p = 2.0$, which are shown in Fig. 5 (i) and (ii). This confirms the existence of only two edge states in system. Similar scenarios are also found in other two cases of Fig. 2(not shown).

Up to this point, it is understood that the system for different choices of the unit cells exhibits different gapped phases, and some of these gapped phases host zero-energy edge states. While these signatures hint towards the topological phases, to concretely characterize the topological nature of the bulk, we compute the Zak phase [21, 22], which serves as the relevant bulk topological invariant for the present one-dimensional system.

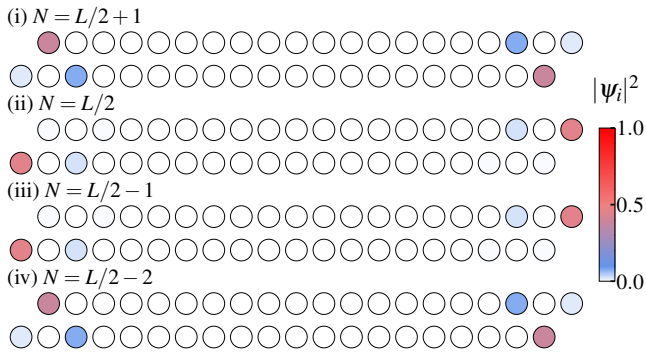


FIG. 4. On-site probability density $|\psi_i|^2$ of four states located at the center of the spectrum for a system of size $L = 40$ sites at $t_p = 0.5$.

The Zak phase is evaluated numerically as

$$\nu = -\Im \ln \prod_{j=0}^{N-1} \det(\langle u_{m,k_j} | u_{n,k_{j+1}} \rangle), \quad (3)$$

where \Im denotes the imaginary part. Here, $k_j = 2\pi j/(Na)$ represents the j th momentum point in the Brillouin zone, a is the lattice spacing, and $|u_{m,k_j}\rangle$ denotes the cell-periodic part of the Bloch eigenstate corresponding to the occupied band m at momentum k_j . The determinant is taken to properly account for the multiband nature of the occupied subspace. A trivial insulating phase is characterized by $\nu = 0$, whereas a topologically nontrivial phase corresponds to $\nu = \pi$. The Zak phase, calculated as a function of t_p , is shown by green circles in the bottom panels of Fig. 2. For the uniform dimerization configuration, a gapped phase hosting a single pair of zero-energy states is characterized by $\nu/\pi = 1$. Upon increasing t_p , the bulk gap closes, rendering the Zak phase ill-defined. As the gap reopens at $t_p > t_p^c$, we get the Zak phase $\nu/\pi = 1$ which corresponds to the two zero energy edge states. For unit cell 2 of the staggered dimerization configuration, we obtain $\nu/\pi = 2$ which corresponds to two pairs of zero-energy edge states for $t_p < t_p^c$. These states merge with the bulk at $t_p = t_p^c$ where the bulk gap closes. Upon gap reopening ($t_p > t_p^c$),

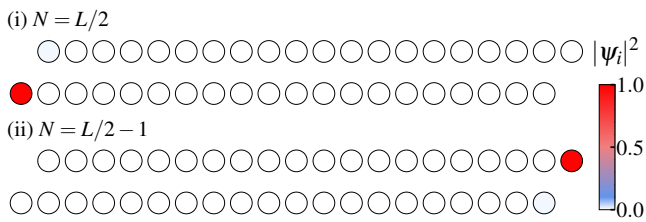


FIG. 5. On-site probability densities $|\psi_i|^2$ of two states located at the center of the spectrum for a system of size $L = 40$ sites at $t_p = 2.0$.

a single pair of zero-energy edge states survives, accompanied by a reduction of the Zak phase to $\nu/\pi = 1$. In contrast, unit cell 3 of the staggered configuration exhibits a vanishing Zak phase at $t_p < t_p^c$ which matches with absence of any edge states. This confirms the trivial nature of the gapped phase in this region of t_p . However, increasing t_p results in a finite Zak phase of $\nu/\pi = 1$ for $t_p > t_p^c$. This corresponds to the appearance of a pair of zero-energy edge states in the spectrum. These results demonstrate a direct correspondence between the bulk Zak phase and the emergence of zero-energy mid-gap edge states, confirming the topological nature of the phases and phase transitions.

At this point, we want to comment that even though one chooses different unit cell configurations, the bulk property will remain the same, and hence the band structure. All the bulk Hamiltonians are equivalent to each other up to a unitary transformation. In the following, we explicitly show few of them. Corresponding to the unit cell highlighted using the red box for both uniform and staggered configuration (in Fig. 1), the Fourier space Hamiltonian is given by

$$H_{1u} = \begin{pmatrix} 0 & -t_p & 0 & \mu_1 \\ -t_p & 0 & \mu_1 & 0 \\ 0 & \mu_1^* & 0 & -t_p \\ \mu_1^* & 0 & -t_p & 0 \end{pmatrix} \quad (4)$$

and

$$H_{1s} = \begin{pmatrix} 0 & -t_p & 0 & \mu_2 \\ -t_p & 0 & \mu_3 & 0 \\ 0 & \mu_3^* & 0 & -t_p \\ \mu_2^* & 0 & -t_p & 0 \end{pmatrix} \quad (5)$$

where we have set the lattice constant to unity, with $\mu_1 = -t_2 - t_1 e^{-ik}$, $\mu_2 = -t_1 - t_2 e^{-ik}$, and $\mu_3 = -t_2 - t_1 e^{-ik}$ with k representing the quasi-momentum. Similarly, the Fourier space Hamiltonian corresponding to the unit cell highlighted by the blue box, corresponding to uniform and staggered configurations are given by

$$H_{2u} = \begin{pmatrix} 0 & 0 & -t_p & \mu_3 \\ 0 & 0 & \mu_2 & -t_p e^{-ik} \\ -t_p & \mu_2^* & 0 & 0 \\ \mu_3^* & -t_p e^{ik} & 0 & 0 \end{pmatrix} \quad (6)$$

and

$$H_{2s} = \begin{pmatrix} 0 & 0 & -t_p & \mu_1 \\ 0 & 0 & \mu_1 & -t_p e^{-ik} \\ -t_p & \mu_1^* & 0 & 0 \\ \mu_1^* & -t_p e^{ik} & 0 & 0 \end{pmatrix} \quad (7)$$

respectively. Both H_{1s} and H_{2s} are equivalent to each other up to a unitary transformation given by $U_{12s} H_{1s} U_{12s}^\dagger = H_{2s}$. Also, H_{1u} and H_{2u} are equivalent to each other up to a unitary transformation given by

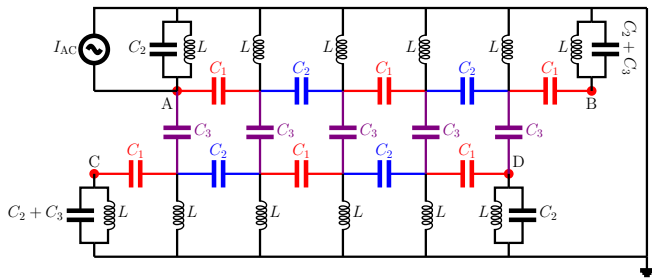


FIG. 6. Schematics of the SSH ladder topoelectrical circuit in a staggered dimerization configuration. Each unit cell consists of three capacitors, C_1 , C_2 , and C_3 , connected by identical inductors L between neighboring capacitors. The circuit is driven by an AC current source with amplitude I_{AC} . Unit-cell configurations 2 and 3 are realized by tuning the capacitance ratio C_1/C_2 to values smaller than or larger than unity. Nodes specified by A, B, C, and D are the nodes where we measure the impedance.

$U_{12u} H_{1u} U_{12u}^\dagger = H_{2u}$, where

$$U_{12s} = U_{12u} = \begin{pmatrix} 1 & 0 & 0 & 0 \\ 0 & 0 & e^{-ik} & 0 \\ 0 & 1 & 0 & 0 \\ 0 & 0 & 0 & 1 \end{pmatrix} \quad (8)$$

In an analogous manner, one can show that the bulk Hamiltonian associated with unit cell 3 (highlighted by the magenta box) is unitarily equivalent to the bulk Hamiltonians indicated by the red and blue boxes for the respective configurations. The same conclusion also holds for the uniform dimerization configuration shown in the left panel of Fig. 1.

In the following, we discuss the LC circuit model that is used to simulate all the above phenomena.

A. Topo-Electric circuit simulation

After getting insights on the topological phases and various edge states properties, we now perform an experimental simulation of our findings using topoelectric circuit simulations. Topo-electric circuits have recently emerged as a very simple, yet powerful and flexible platform for simulating topological phenomena in tight-binding lattices [23]. The peculiar similarity between the quantum lattice model and the circuit Laplacian provides an interesting avenue to map the Hamiltonian matrix to the admittance matrix. As a result the eigenstates of the quantum model can be viewed as the voltage response across different nodes. These systems offer several key advantages, including precise control over parameters, direct access to edge responses via impedance measurements, and the ability to simulate both Hermitian and non-Hermitian topological phases [24–35]. Due to such properties, topo-electric circuits have recently attracted a great deal of attention to observe topological phases in various geometries [36]. Importantly, circuit realizations

of SSH-type models have demonstrated clear signatures of topological boundary modes, providing an experimentally accessible route to visualize bulk-boundary correspondence in real space [37].

We consider the situation shown in Fig. 2 (b) to capture the topological features under OBC which corresponds to the unit cell configuration 2 in Fig. 1 (right panel). The lattice model for this configuration under OBC (Fig. 1(a3)) can be mapped into a circuit model as depicted in Fig. 6. Although for numerical purposes we consider larger systems, we use a smaller circuit of 5 cells for the following discussion. The hopping dimerization in each leg t_1 and t_2 can be achieved by considering capacitors with alternating capacitances C_1 and C_2 , respectively. The inter-leg coupling t_p is achieved by using another capacitor of capacitance C_3 . The junction between the capacitors in each legs are connected by inductors L which are grounded. In addition, we also add extra capacitors to the edge nodes to match their onsite potentials with the bulk nodes as depicted in Fig. 6. Following Kirchoff's law, the eigen equation corresponding to the above circuit can be written as

$$\mathbf{I} = (L + W)\mathbf{V} \equiv \mathbf{J}\mathbf{V}, \quad (9)$$

where \mathbf{V} and \mathbf{I} are vectors composed of the node voltages and injected nodal currents. Here the grounded Laplacian J is the sum of the circuit Laplacian L , which encodes the network structure, and the diagonal matrix (W) specifies the grounding configuration, which in our case is given by

$$W = i\omega \text{Diag} \left(C_2 - \frac{1}{\omega^2 L}, -\frac{1}{\omega^2 L}, -\frac{1}{\omega^2 L}, -\frac{1}{\omega^2 L}, -\frac{1}{\omega^2 L}, \right. \\ \left. C_1 + C_2 - \frac{1}{\omega^2 L}, C_1 + C_2 - \frac{1}{\omega^2 L}, -\frac{1}{\omega^2 L}, -\frac{1}{\omega^2 L}, \right. \\ \left. -\frac{1}{\omega^2 L}, -\frac{1}{\omega^2 L}, C_2 - \frac{1}{\omega^2 L} \right). \quad (10)$$

The circuit Laplacian

$$L = D - C, \quad (11)$$

with C and D being the adjacency and the degree matrices, respectively (See Appendix A). With these ingredients in hand, we derive the associated Laplacian to our grounded circuit as

$$J = i\omega \begin{pmatrix} D & -C_1 & 0 & 0 & 0 & \dots & -C_3 & 0 & 0 & 0 & 0 \\ -C_1 & D & -C_2 & 0 & 0 & \dots & 0 & -C_3 & 0 & 0 & 0 \\ 0 & -C_2 & D & -C_1 & 0 & \dots & 0 & 0 & -C_3 & 0 & 0 \\ 0 & 0 & -C_1 & D & -C_2 & \dots & 0 & 0 & 0 & -C_3 & 0 \\ 0 & 0 & 0 & -C_2 & D & \dots & 0 & 0 & 0 & 0 & -C_3 \\ 0 & 0 & 0 & 0 & -C_1 & \dots & 0 & 0 & 0 & 0 & 0 \\ 0 & 0 & 0 & 0 & 0 & \dots & -C_1 & 0 & 0 & 0 & 0 \\ -C_3 & 0 & 0 & 0 & 0 & \dots & D & -C_2 & 0 & 0 & 0 \\ 0 & -C_3 & 0 & 0 & 0 & \dots & -C_2 & D & -C_1 & 0 & 0 \\ 0 & 0 & -C_3 & 0 & 0 & \dots & 0 & -C_1 & D & -C_2 & 0 \\ 0 & 0 & 0 & -C_3 & 0 & \dots & 0 & 0 & -C_2 & D & -C_1 \\ 0 & 0 & 0 & 0 & -C_3 & \dots & 0 & 0 & 0 & -C_1 & D \end{pmatrix}$$

with $D = C_1 + C_2 + C_3 - \frac{1}{\omega^2 L}$. Now setting $D = 0$, we

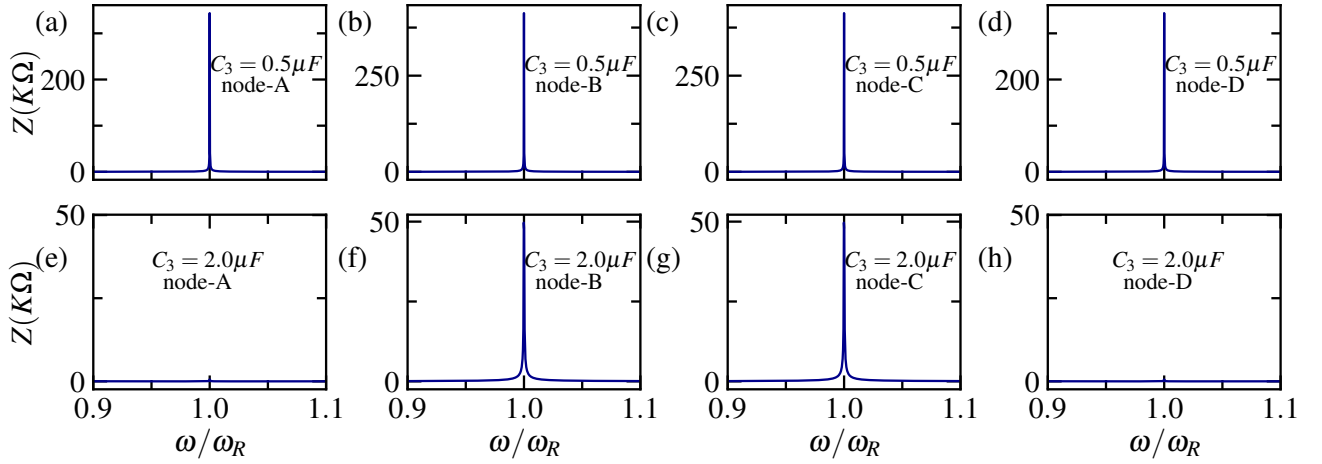


FIG. 7. Impedance $Z(K\Omega)$ measured across all the edge nodes as a function of normalized AC frequency ω/ω_R for a circuit made out of 50 cells. The circuit parameters are set to $C_1 = 0.2\mu F$, $C_2 = 1\mu F$, and $L = 1mH$. (a-d) Show the impedances $C_3 = 0.5\mu F$ and (e-f) for $C_3 = 2.0\mu F$.

get the resonant frequency associated with the circuit as

$$\omega_R = \frac{1}{\sqrt{L(C_1 + C_2 + C_3)}}. \quad (12)$$

Using the above circuit configuration, we probe the topological signatures through impedance measurements using LTspice simulations [36, 38–42]. We measure the two-point impedance [43, 44] given by $Z_{mn} = (V_m - V_n)/I$, where m and n represent the nodes among which the voltage difference is being calculated, and I represents the externally injected AC current flowing from node- m to node- n . A pronounced peak in the impedance indicates that the admittance matrix possesses at least one eigenvalue that is close to zero. In the circuit realization of the topologically non-trivial phases, such a strong response is a signature of gapless boundary modes associated with a topologically nontrivial phase [45]. To identify the emergence of edge modes for the configuration shown in Fig. 6, we inject current at the edge nodes marked as A, B, C, and D in Fig. 6 and measure the voltage difference with respect to the ground.

For the case under consideration, we expect to observe a phase transition from a topological phase possessing four edge states to another topological phase with two edge states. To obtain the signatures of four edge states, which occurs in the limit of weak inter-leg coupling, we choose the circuit parameters as $C_1 = 0.2\mu F$, $C_2 = 1\mu F$, $C_3 = 0.5\mu F$, and $L = 1mH$ and plot the two point impedance Z as a function of normalized angular frequency ω/ω_R in the upper panel of Fig. 7. With the choice of the above parameters, the computed resonance frequency using Eq. 12 is obtained as $f = \omega_R/2\pi = 3.860$ kHz. Our simulation shows prominent impedance peaks at nodes A, B, C, and D, indicating the presence of four zero-energy modes. For the case of strong inter-leg coupling, we choose $C_1 = 0.2\mu F$, $C_2 = 1\mu F$, $C_3 = 2\mu F$,

and $L = 1mH$ and plot Z in units of $K\Omega$ as a function of normalized angular frequency ω/ω_R in the lower panel of Fig. 7. Now, the resonance frequency shifts to $f = 2.813$ kHz. In this regime, two impedance peaks are observed only at nodes B and C, whereas no peaks are observed at nodes A and D. To further complement these observations, we probe the voltage response (V) which is equivalent to the probability amplitudes of the tight binding model given in Eq. (1). To this end, we apply a sinusoidal excitation of frequency $f = 3.860$ kHz, and measure the voltage response across all the nodes which are plotted in Fig. 8. The voltage distribution revealed strong localization of the zero energy mode at all the terminal nodes, which agrees well with the numerical prediction that there exist four edge states in this parameter regime. On the other hand, when excited at $f = 2.813$ kHz, the voltage distribution shows localization at the two edge nodes as shown in Fig. 9. The

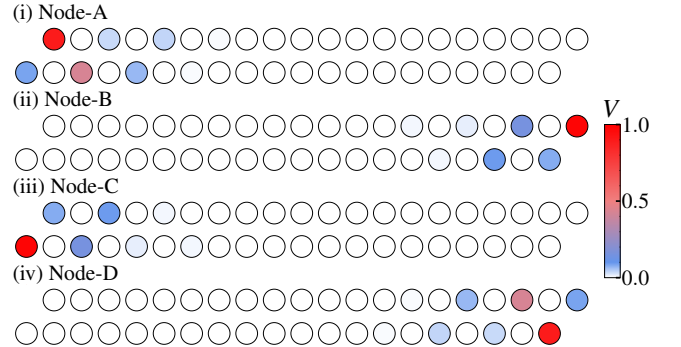


FIG. 8. Depicts the local voltage distribution of all four edge excitations with the circuit parameters set to $C_1 = 0.2\mu F$, $C_2 = 1\mu F$, $C_3 = 0.5\mu F$ and $L = 1mH$.

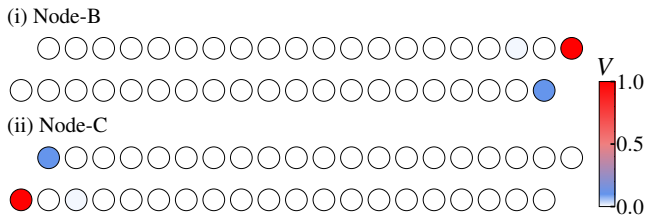


FIG. 9. Depicts the local voltage distribution (V) of all four edge excitations with the circuit parameters set to $C_1 = 0.2\mu F$, $C_2 = 1\mu F$, $C_3 = 2.0\mu F$ and $L = 1mH$.

simulation results show excellent agreement with theoretical predictions. Similar signatures are obtained for the topological phases of other unit cell configurations (not shown).

IV. CONCLUSION

In this work, we investigated a two-leg SSH ladder and demonstrated the emergence of tunable topological phases, phase transitions, and edge state engineering by appropriately defining the unit-cell configuration. We showed that these topological phases exhibit different bulk-boundary correspondence, allowing for possible edge state engineering. We proposed a topoelectric circuit simulations to observe these signatures through impedance measurements and the voltage response of the circuit. The existence of topological edge states was verified through impedance signatures and voltage distribution profiles obtained from circuit analysis via LTspice simulations. These findings highlight the potential of topoelectrical circuits as experimentally accessible realizations of lattice topological phases and open avenues for investigating disorder effects, higher-dimensional circuit architectures and non-Hermitian environment.

V. ACKNOWLEDGMENT

We thank Biswajit Paul for useful discussions. T.M. acknowledges support from Science and Engineering Research Board (SERB), Govt. of India, through project No. MTR/2022/000382 and STR/2022/000023.

Appendix A: Additional Details

We design the electrical circuit from the weighted graph where we take each vertices as circuit nodes and weighted edges as linear circuit components with edge weights as admittance of that circuit components. While we choose capacitors as edges in our circuit, one is free to choose inductive edges which does not change the overall circuit features. The weighted adjacency matrix C is the

matrix of admittances corresponding to our circuit, and the matrix elements can be defined as

$$C_{ij} = \begin{cases} Y_{ij} & \text{if vertices } i \text{ and } j \text{ are connected, } i \neq j \\ 0 & \text{otherwise,} \end{cases}$$

where Y_{ij} denotes the admittance of the circuit element connecting nodes i and j . For the three types of couplings in our circuit, the admittances are given by $i\omega C_1$, $i\omega C_2$, and $i\omega C_3$, depending on the corresponding capacitor in the network. So, the adjacency matrix for our circuit with 3 types of couplings made by analogy with the tight-binding lattice will be,

$$C = i\omega \begin{pmatrix} 0 & C_1 & 0 & 0 & 0 & 0 & 0 & C_3 & 0 & 0 & 0 & 0 \\ C_1 & 0 & C_2 & 0 & 0 & 0 & 0 & 0 & C_3 & 0 & 0 & 0 \\ 0 & C_2 & 0 & C_1 & 0 & 0 & 0 & 0 & 0 & C_3 & 0 & 0 \\ 0 & 0 & C_1 & 0 & C_2 & 0 & 0 & 0 & 0 & 0 & C_3 & 0 \\ 0 & 0 & 0 & C_2 & 0 & C_1 & 0 & 0 & 0 & 0 & 0 & C_3 \\ 0 & 0 & 0 & 0 & C_1 & 0 & 0 & 0 & 0 & 0 & 0 & 0 \\ 0 & 0 & 0 & 0 & 0 & 0 & 0 & C_1 & 0 & 0 & 0 & 0 \\ C_3 & 0 & 0 & 0 & 0 & 0 & C_1 & 0 & C_2 & 0 & 0 & 0 \\ 0 & C_3 & 0 & 0 & 0 & 0 & 0 & C_2 & 0 & C_1 & 0 & 0 \\ 0 & 0 & C_3 & 0 & 0 & 0 & 0 & C_1 & 0 & C_2 & 0 & 0 \\ 0 & 0 & 0 & C_3 & 0 & 0 & 0 & 0 & C_2 & 0 & C_1 & 0 \\ 0 & 0 & 0 & 0 & C_3 & 0 & 0 & 0 & 0 & 0 & C_1 & 0 \end{pmatrix}$$

From the coupling matrix C , we now define the degree matrix D , which contains the total admittances from each node towards the rest of the circuit and is a diagonal matrix whose diagonal entries are given by the total weight connected to each vertex,

$$D_{ii} = \sum_{i=1}^N C_{ij}$$

and $D_{ij} = 0$, for $i \neq j$. The degree matrix for this weighted graph will be a diagonal matrix and is given by

$$D = i\omega \begin{pmatrix} C' & 0 & 0 & 0 & 0 & 0 & 0 & 0 & 0 & 0 & 0 & 0 \\ 0 & C & 0 & 0 & 0 & 0 & 0 & 0 & 0 & 0 & 0 & 0 \\ 0 & 0 & C & 0 & 0 & 0 & 0 & 0 & 0 & 0 & 0 & 0 \\ 0 & 0 & 0 & C & 0 & 0 & 0 & 0 & 0 & 0 & 0 & 0 \\ 0 & 0 & 0 & 0 & C & 0 & 0 & 0 & 0 & 0 & 0 & 0 \\ 0 & 0 & 0 & 0 & 0 & C_1 & 0 & 0 & 0 & 0 & 0 & 0 \\ 0 & 0 & 0 & 0 & 0 & 0 & C_1 & 0 & 0 & 0 & 0 & 0 \\ 0 & 0 & 0 & 0 & 0 & 0 & 0 & C & 0 & 0 & 0 & 0 \\ 0 & 0 & 0 & 0 & 0 & 0 & 0 & 0 & C & 0 & 0 & 0 \\ 0 & 0 & 0 & 0 & 0 & 0 & 0 & 0 & 0 & C & 0 & 0 \\ 0 & 0 & 0 & 0 & 0 & 0 & 0 & 0 & 0 & 0 & C & 0 \\ 0 & 0 & 0 & 0 & 0 & 0 & 0 & 0 & 0 & 0 & 0 & C' \end{pmatrix}$$

where $C = C_1 + C_2 + C_3$ and $C' = C_1 + C_3$. As bulk vertices are connected to two intra-chain neighbors and one inter-chain neighbor, their diagonal entries are in the form of $D_{ii} = i\omega(C_1 + C_2 + C_3)$. In contrast, boundary vertices have fewer connections, leading to fewer contribution terms because of the open boundary condition chosen.

The matrices C and D define the graph Laplacian, $L = D - C$, which forms the target operator to be implemented in the electrical circuit and is given as .

$$L = i\omega \begin{pmatrix} C' & -C_1 & 0 & 0 & 0 & 0 & 0 & -C_3 & 0 & 0 & 0 & 0 \\ -C_1 & C & -C_2 & 0 & 0 & 0 & 0 & 0 & -C_3 & 0 & 0 & 0 \\ 0 & -C_2 & C & -C_1 & 0 & 0 & 0 & 0 & 0 & -C_3 & 0 & 0 \\ 0 & 0 & -C_1 & C & -C_2 & 0 & 0 & 0 & 0 & 0 & -C_3 & 0 \\ 0 & 0 & 0 & -C_2 & C & -C_1 & 0 & 0 & 0 & 0 & 0 & -C_3 \\ 0 & 0 & 0 & 0 & -C_1 & C_1 & 0 & 0 & 0 & 0 & 0 & 0 \\ 0 & 0 & 0 & 0 & 0 & 0 & C_1 & -C_1 & 0 & 0 & 0 & 0 \\ -C_3 & 0 & 0 & 0 & 0 & 0 & -C_1 & C & -C_2 & 0 & 0 & 0 \\ 0 & -C_3 & 0 & 0 & 0 & 0 & 0 & -C_2 & C & -C_1 & 0 & 0 \\ 0 & 0 & -C_3 & 0 & 0 & 0 & 0 & 0 & -C_1 & C & -C_2 & 0 \\ 0 & 0 & 0 & -C_3 & 0 & 0 & 0 & 0 & 0 & -C_2 & C & -C_1 \\ 0 & 0 & 0 & 0 & -C_3 & 0 & 0 & 0 & 0 & 0 & -C_1 & C' \end{pmatrix}$$

The Laplacian L is independent of any choice of grounding and corresponds to a floating network.

To define absolute node voltages and impedance measurement, the circuit must be grounded. All the grounding terms will appear at the diagonal of J . Grounding through inductors will give us a choice to cancel the on-site admittance terms at a particular frequency, just like how we set on-site potentials to be zero, we will call that frequency the resonant frequency. For this cancellation to happen, we need extra capacitors to ground from edge nodes, as they lack some connections due to finite chain boundaries. The resulting circuit is as already shown, becomes Fig. 6.

-
- [1] W. P. Su, J. R. Schrieffer, and A. J. Heeger, Solitons in polyacetylene, *Phys. Rev. Lett.* **42**, 1698 (1979).
- [2] M. Atala, M. Aidelsburger, J. T. Barreiro, D. Abanin, T. Kitagawa, E. Demler, and I. Bloch, Direct measurement of the zak phase in topological bloch bands, *Nature Physics* **9**, 795 (2013).
- [3] S. Nakajima, T. Tomita, S. Taie, T. Ichinose, H. Ozawa, L. Wang, M. Troyer, and Y. Takahashi, Topological thouless pumping of ultracold fermions, *Nature Physics* **12**, 296 (2016).
- [4] M. Lohse, C. Schweizer, O. Zilberberg, M. Aidelsburger, and I. Bloch, A thouless quantum pump with ultracold bosonic atoms in an optical superlattice, *Nature Physics* **12**, 350 (2016).
- [5] S. Mukherjee, A. Spracklen, M. Valiente, E. Andersson, P. Öhberg, N. Goldman, and R. R. Thomson, Experimental observation of anomalous topological edge modes in a slowly driven photonic lattice, *Nature Communications* **8**, 13918 (2017).
- [6] L. Lu, J. D. Joannopoulos, and M. Soljačić, Topological photonics, *Nature Photonics* **8**, 821 (2014).
- [7] L. Thatcher, P. Fairfield, L. Merlo-Ramírez, and J. M. Merlo, Experimental observation of topological phase transitions in a mechanical 1d-ssh model, *Physica Scripta* **97**, 035702 (2022).
- [8] E. J. Meier, F. A. An, and B. Gadway, Observation of the topological soliton state in the su–schrieffer–heeger model, *Nature Communications* **7**, 13986 (2016).
- [9] D. Xie, W. Gou, T. Xiao, B. Gadway, and B. Yan, Topological characterizations of an extended su–schrieffer–heeger model, *npj Quantum Information* **5**, 55 (2019).
- [10] T. Kitagawa, M. A. Broome, A. Fedrizzi, M. S. Rudner, E. Berg, I. Kassal, A. Aspuru-Guzik, E. Demler, and A. G. White, Observation of topologically protected bound states in photonic quantum walks, *Nature Communications* **3**, 882 (2012).
- [11] M. Leder, C. Grossert, L. Sitta, M. Genske, A. Rosch, and M. Weitz, Real-space imaging of a topologically protected edge state with ultracold atoms in an amplitude-chirped optical lattice, *Nature Communications* **7**, 13112 (2016).
- [12] S. de Léséleuc, V. Lienhard, P. Scholl, D. Barredo, S. Weber, N. Lang, H. P. Büchler, T. Lahaye, and A. Browaeys, Observation of a symmetry-protected topological phase of interacting bosons with rydberg atoms, *Science* **365**, 775 (2019).
- [13] N. H. Le, A. J. Fisher, N. J. Curson, and E. Ginossar, Topological phases of a dimerized fermi–hubbard model for semiconductor nano-lattices, *npj Quantum Information* **6**, 24 (2020).
- [14] C. Jörg, M. Jürgensen, S. Mukherjee, and M. C. Rechtsman, Optical control of topological end states via soliton formation in a 1d lattice, *Nanophotonics* doi:10.1515/nanoph-2024-0401 (2024).
- [15] Y. Liu, Y.-R. Zhang, Y.-H. Shi, T. Liu, C. Lu, Y.-Y. Wang, H. Li, T.-M. Li, C.-L. Deng, S.-Y. Zhou, T. Liu, J.-C. Zhang, G.-H. Liang, Z.-Y. Mei, W.-G. Ma, H.-T. Liu, Z.-H. Liu, C.-T. Chen, K. Huang, X. Song, S. P. Zhao, Y. Tian, Z. Xiang, D. Zheng, F. Nori, K. Xu, and H. Fan, Interplay between disorder and topology in thouless pumping on a superconducting quantum processor, *Nature Communications* **16**, 108 (2025).
- [16] X. Wu, X. Liang, Y. Tian, F. Yang, C. Chen, Y.-C. Liu, M. K. Tey, and L. You, A concise review of rydberg atom based quantum computation and quantum simulation*, *Chinese Physics B* **30**, 020305 (2021).
- [17] Y. Liu, W. Cao, W. Chen, H. Wang, L. Yang, and X. Zhang, Fully integrated topological electronics, *Scientific Reports* **12**, 13410 (2022).
- [18] C. H. Lee, S. Imhof, C. Berger, F. Bayer, J. Brehm, L. W. Molenkamp, T. Kiessling, and R. Thomale, Topoelectrical circuits, *Communications Physics* **1**, 39 (2018).
- [19] R. Parida, B. Paul, S. R. Padhi, and T. Mishra, *Coupling induced emergent topology in a two-leg fermionic ladder* (2025), arXiv:2509.25130 [cond-mat.quant-gas].
- [20] A. Padhan, S. Mondal, S. Vishveshwara, and T. Mishra, Interacting bosons on a su–schrieffer–heeger ladder: Topological phases and thouless pumping, *Phys. Rev. B* **109**, 085120 (2024).
- [21] M. V. Berry, Quantal phase factors accompanying adiabatic changes, *Proc. Roy. Soc. London A* **392**, 45 (1984).
- [22] J. Zak, Berry’s phase for energy bands in solids, *Phys. Rev. Lett.* **62**, 2747 (1989).
- [23] T. Helbig, T. Hofmann, C. H. Lee, R. Thomale, S. Imhof, L. W. Molenkamp, and T. Kiessling, Band structure engineering and reconstruction in electric circuit networks, *Phys. Rev. B* **99**, 161114 (2019).
- [24] M. Ezawa, Braiding of majorana-like corner states in electric circuits and its non-hermitian generalization, *Phys. Rev. B* **100**, 045407 (2019).

- [25] L. Li, C. H. Lee, S. Mu, and J. Gong, Critical non-hermitian skin effect, *Nature Communications* **11**, 5491 (2020).
- [26] T. Hofmann, T. Helbig, F. Schindler, N. Salgo, M. Brzezińska, M. Greiter, T. Kiessling, D. Wolf, A. Vollhardt, A. Kabaši, C. H. Lee, A. Bilušić, R. Thomale, and T. Neupert, Reciprocal skin effect and its realization in a topoelectrical circuit, *Phys. Rev. Res.* **2**, 023265 (2020).
- [27] T. Helbig, T. Hofmann, S. Imhof, M. Abdelghany, T. Kiessling, L. W. Molenkamp, C. H. Lee, A. Szameit, M. Greiter, and R. Thomale, Generalized bulk–boundary correspondence in non-hermitian topoelectrical circuits, *Nature Physics* **16**, 747 (2020).
- [28] S. M. Rafi-Ul-Islam, Z. B. Siu, H. Sahin, C. H. Lee, and M. B. A. Jalil, Unconventional skin modes in generalized topoelectrical circuits with multiple asymmetric couplings, *Phys. Rev. Res.* **4**, 043108 (2022).
- [29] H. Zhang, T. Chen, L. Li, C. H. Lee, and X. Zhang, Electrical circuit realization of topological switching for the non-hermitian skin effect, *Phys. Rev. B* **107**, 085426 (2023).
- [30] S. Ganguly and S. K. Maiti, Electrical analogue of one-dimensional and quasi-one-dimensional aubry–andr e–harper lattices, *Scientific Reports* **13**, 13633 (2023).
- [31] A. Stegmaier, S. Imhof, T. Helbig, T. Hofmann, C. H. Lee, M. Kremer, A. Fritzsche, T. Feichtner, S. Klemmt, S. H ofling, I. Boettcher, I. C. Fulga, L. Ma, O. G. Schmidt, M. Greiter, T. Kiessling, A. Szameit, and R. Thomale, Topological defect engineering and \mathcal{PT} symmetry in non-hermitian electrical circuits, *Phys. Rev. Lett.* **126**, 215302 (2021).
- [32] S. Imhof, C. Berger, F. Bayer, J. Brehm, L. W. Molenkamp, T. Kiessling, F. Schindler, C. H. Lee, M. Greiter, T. Neupert, and R. Thomale, Topoelectrical-circuit realization of topological corner modes, *Nature Physics* **14**, 925 (2018).
- [33] H. Yuan, W. Zhang, Z. Zhou, W. Wang, N. Pan, Y. Feng, H. Sun, and X. Zhang, Non-hermitian topoelectrical circuit sensor with high sensitivity, *Advanced Science* **10**, 2301128 (2023).
- [34] S. M. Rafi-Ul-Islam, Z. B. Siu, M. S. H. Razo, and M. B. Jalil, Localization control of defect states via non-hermitian effects in topoelectrical circuits, *Advanced Quantum Technologies* **n/a**, e00687.
- [35] D. Halder, R. Thomale, and S. Basu, Circuit realization of a two-orbital non-hermitian tight-binding chain, *Phys. Rev. B* **109**, 115407 (2024).
- [36] J. Dong, V. Juri c, and B. Roy, Topoelectric circuits: Theory and construction, *Phys. Rev. Res.* **3**, 023056 (2021).
- [37] H. Sahin, M. B. A. Jalil, and C. H. Lee, Topoelectrical circuits—recent experimental advances and developments, *APL Electronic Devices* **1**, 021503 (2025).
- [38] C. H. Lee, S. Imhof, C. Berger, F. Bayer, J. Brehm, L. W. Molenkamp, T. Kiessling, and R. Thomale, Topoelectrical circuits, *Communications Physics* **1**, 39 (2018).
- [39] T. Kotwal, F. Moseley, A. Stegmaier, S. Imhof, H. Brand, T. Kie bling, R. Thomale, H. Ronellenfisch, and J. Dunkel, Active topoelectrical circuits, *Proceedings of the National Academy of Sciences* **118**, e2106411118 (2021).
- [40] L. Zhang, B. Ruan, and X. Dai, Bound states in the continuum of three-leg ladder topoelectrical circuits, *Journal of Applied Physics* **137**, 095104 (2025).
- [41] N. S. Izmailian and R. Kenna, A generalised formulation of the laplacian approach to resistor networks, *Journal of Statistical Mechanics: Theory and Experiment* **2014**, P09016 (2014).
- [42] N. S. Izmailian, R. Kenna, and F. Y. Wu, The two-point resistance of a resistor network: a new formulation and application to the cobweb network, *Journal of Physics A: Mathematical and Theoretical* **47**, 035003 (2013).
- [43] F. Y. Wu, Theory of resistor networks: the two-point resistance, *Journal of Physics A: Mathematical and General* **37**, 6653 (2004).
- [44] W. J. Tzeng and F. Y. Wu, Theory of impedance networks: the two-point impedance and lc resonances, *Journal of Physics A: Mathematical and General* **39**, 8579 (2006).
- [45] H. Sahin, Z. B. Siu, S. M. Rafi-Ul-Islam, J. F. Kong, M. B. A. Jalil, and C. H. Lee, Impedance responses and size-dependent resonances in topoelectrical circuits via the method of images, *Phys. Rev. B* **107**, 245114 (2023).